33rd Annual International Conference of the IEEE EMBS
Boston, Massachusetts USA, August 30 - September 3, 2011

Neural Decoding Using Local Field Potential Based On Partial Least Squares Regression

Rui Wang, Xinxin Lou, Bo Jiang, Weidong Cheng, Xiaoxiang Zheng, Shaomin Zhang *

Abstract—**Recent studies have shown that a promising cortical control signal in brain-machine interface is local field potential (LFP), of which low and high frequencies bands contains information about planning or executing dexterous movement. In this paper, we analyzed LFP signals recorded from primary motor cortex of rats as they performed a lever-pressing task. The decoding performance of partial least squares regression (PLSR) in LFP was evaluated by comparing with two traditional decoding algorithms, Wiener filtering (WF) and Kalman filtering (KF). The results demonstrated that PLSR not only had good performance as the other two methods, but also had particular predominance in avoiding over-fitting and computation complexity, due to its capability in dealing with the small sample capacity and high variable dimension that exist in LFP decoding.**

I. Introduction

THE technology of brain-machine interfaces (BMIs) enable a brain to direct control an external device, considered as a means of assisting or repairing human cognitive or sensory-motor functions [1-3]. Plenty of studies on non-human primate have demonstrated that the neural signals recorded from motor cortex had been successfully used as control signal to control 2D or 3D cursors, even a 4-DOF robotic arm [4-6].

The action potentials (spike), by reason that its recordings are richer in formation and offer a higher degrees of freedom, was most commonly used in invasive BMIs. Several signals processing methods have acquired good result in decoding from spike signals, such as linear or nonlinear regression. Because of its susceptibility to encapsulation issues, however, spike is not stable over time [7].

Local field potential (LFP), another type of neural signals, attracted much attention recently, although it had been ignored in previous decoding studies. Researchers demonstrated that the trajectory of dexterous movement of the arm and hand could be finely predicted by different frequency components of LFP signals [8, 9]. LFP would be a promising cortical control signal for BMIs. In contrast with spike, only a few studies were carried on the LFP decoding algorithms.

Partial least squares regression (PLSR) can implement modeling, predigesting and correlation analysis simultaneously. It had performed well in decoding of arm motion from electrocorticographic (ECoG) signals in monkeys and 3D finger trajectories from echoencephalographic (EEG) signals in human [10,11]. These studies suggested it had promising potential in decoding continuous neural signals.

In this study, we recorded the LFP signals form motor cortex of rats when they were trained to perform a lever-pressing task with their forelimbs. We analyzed the relationship of LFP signals in different frequency bands and in different channels. Meanwhile, PLSR and two commonly-used decoding methods, Wiener filtering (WF) and Kalman filtering (KF), were used to predict the kinematics of forelimb respectively. The performances of these three decoding algorithms were evaluated.

II. Methods

A. Behavioral Task and Animal Surgery

All recordings were from five male Sprague-Dawley rats (weighing 275-300g) using protocols approved by the Animal Care Committee at Zhejiang University, China, that follows the Care and Use of Laboratory Animals (China Ministry of Health). Rats were randomly labeled as R1, R2, R3, R4 and R5, and performed operant conditional task. Each rat was placed in an operant chamber and required to press a lever down to a certain level for water rewards. The rats were deprived of water, and maintained 12mL water per day while trained. They were not implanted until trained to achieve a success rate of >75%. Simultaneous spike and LFP recordings were acquired using 16-channel (2×8) microwire array (California Fine Wire) which implanted in the region of the forelimb in primary motor cortex. The electrode tips were positioned in the layer V whose approximate depth ranged from 1.1mm to 1.8mm beneath the pia in the cerebral cortex. We acquired the neural data from rats after seven or more days of their surgery.

Manuscript received March 26, 2011. This work was supported by the National Science Foundation of China (61031002, 61001172) and Zhejiang provincial key science and technology program for international cooperation(No. 2011C14005)

Rui Wang is with Qiushi Academy of Advanced Studies and College of Biomedical Engineering and College of Biomedical Engineering and Instrumental Science, Zhejiang University, Hangzhou, 310027, PR China. (e-mail: Suriwang1988@gmail.com)

XinXin Lou is with Qiushi Academy of Advanced Studies and College of Biomedical Engineering and College of Biomedical Engineering and Instrumental Science, Zhejiang University, Hangzhou, 310027, PR China. (e-mail: louxinxin2004@gmail.com). Rui Wang and XinXin Lou contributed equally to this work.

Bo Jiang, Weidong Cheng, Xiaoxiang Zheng are with Qiushi Academy of Advanced StudiesZhejiang University, Hangzhou, 310027, PR China.

Shaomin Zhang is with Qiushi Academy for Advanced Studies and College of Biomedical Engineering and Instrumental Science, Zhejiang University, Hangzhou, 310027, PR China. (phone:+86 571 87953860; fax: +86 571 87951676;e-mail: qaas@zju.edu.cn)

B. Data Acquisition

We used a Cerebus multichannel data acquisition system (Blackrock Inc, US) to filter 16 channels of neural signal analogly and recorded them at the 30 kHz sampling rate. For each channel of the signal, frequency components that were not in the range from 0.3Hz to 7.5 kHz were removed by analog filtering. Then we used digital filter to process signals (low pass with cutoff edge at 300Hz, notch filtering at 50Hz), and sampled them at 1000Hz to produce LFP. Pressure on the lever was synchronously sampled at 500 Hz.

C. Data Analysis

1) Multitaper spectral analysis and coherence: The power spectrum of each LFP was obtained by employing a multitaper spectral estimation method [12]. The LFP-LFP coherence $C_{xy}(f)$ was calculated to analysis the coherency between two LFPs, and is defined as:

$$C_{xy}(f) = \frac{S_{xy}(f)}{\sqrt{S_x(f)S_y(f)}} \quad (1)$$

2) LFP Features: The LFP signals were analyzed in time-frequency mode. The time series of LFP were segmented into a sequence of 500*ms* long segment which was 400ms overlapping to subsequent segment. By using multitaper spectral estimation, each segment was then separated into multiple frequency bands. Eight frequency bands were consequently obtained: δ (0.6-4 Hz), θ (4-8 Hz), α (8-15 Hz), β (15-30 Hz), γ1 (30-50 Hz), γ2 (50-100 Hz), γ3 (100-200 Hz), broad high frequency LFP (bhfLFP: 200-300 Hz) that was similar to ones described in [12]. The eight frequency features were binned with a 100ms time bin, and normalized by calculating the standard *z*-score at each frequency band. Due to the association, the motor parameter at time *t* also related to previous neural activities, the features belonging to present time bin *t* were composed by the frequency features of a period between 400ms before the current time *t* to *t* in our study.

3) Decoding Algorithms: To predict the lever pressure, PLSR was used as the decoding algorithm [13].PLSR estimates a lower dimensional latent structure of the input data to avoid over-fitting as well as to reduce the computational complexity. The model of PLSR can be expressed as:

$$\mathrm{M(t)} = \omega_0 + \sum_{i=1}^{H} \omega_i t_i + \varepsilon(t) \quad (2)$$

Where t_i is the PLS latent component, $H \ll M \times L$ is the number of latent components, ω_0 is the intercept, ω_i is the weight for the latent component, and $\varepsilon(t)$ is the residual error. Firstly the original variable space is projected to a latent variable structure. Then the latent variables explain the maximum covariance between the input space and the output space. In the end only few latent variables are enough to explain most variation of the output space.9-fold cross-validation was performed on the training data and the optimal number of PLS components was determined when the predictive error sum of squares (PRESS) reaches the minimal.

WF and KF were also tested for comparison [4, 14]. It makes fitting multiple covariance matrices computationally infeasible because of correlations among the frequency features of LFP channels and the limited amount of training data. Principal Component Analysis (PCA) was used to reduce the dimension of the input variables before WF and KM decoding. We chose *N* PCA components with the first *N* largest eigenvalues containing 90% of the total variance to cope with the ill-conditioned problem of covariance matrices and reduce the dimension.

4) Performance Measurements: The decoding performance was measured by Correlation coefficient (CC) between the predicted and measured pressure values and their mean square error (MSE). To eliminate the dependence of data set selection, 10-fold cross-validation was performed. Friedman Test was used to test significant difference among three methods.

III. Result

A. Characteristic of LFP

We analyzed the frequency spectrum of LFP signals. Figure 1, an example of a LFP channel analysis, indicates that a decrease in spectral power is evident with the increase of frequency. It suggests that most of the power was taken up by the low-frequency features. Consequently, low frequency bands performed the main role of LFP decoding in previous works. It needs to be mentioned that thought the harmonics of 50Hz are still present after filtering the data, but it had no influence on the result because the harmonics of 50Hz are uniformly distributed in signals throughout all channels.

Next, the variation of LFP signal was studied, along with the tendency that how corresponding movement information varied. Figure 2 shows the normalized average power of different frequency bands of LFP (top panel) along the corresponding average pressing event (bottom panel). From the Figure 2 we can see that the trend accorded with [12]. The peaks of different frequency bands emerged at different points around the pressure peak, while the lever pressure

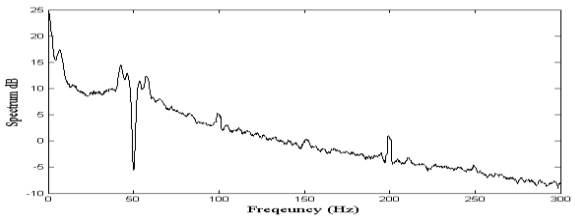

Fig.1. Power spectrum analysis of LFP. Most of the power is taken up by low frequency components. The harmonics of 50Hz did not affect the decoding result, because they are uniformly distributed in signals throughout all channels.

was used as a reference. It is apparent that the power of a high frequency band witnessed its peak after the pressure peak, whereas for low frequency bands the peak arose earlier. Such difference indicated that high frequency bands carried essential information differing from information in the low

frequency bands, thus they can contribute to decoding despite they contained lower power.

We calculated the coherence of LFPs in different channels (Fig. 3.). The results describe that LFPs of different channels become pronounced coherent at low frequency bands, but remarkably dropped from low to high frequencies. It is clear that the coherence among low frequencies from different channels was much higher than high frequencies, revealing

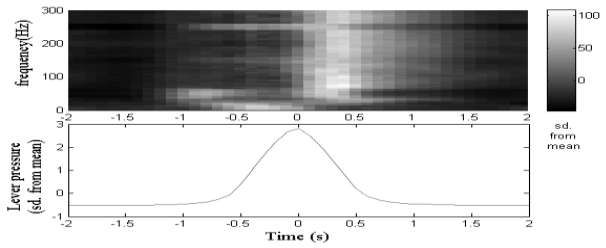

Fig. 2. Normalized average power of all frequency range (top panel), along with the average pressing event (bottom panel) as reference. The low frequency reaches its peak ahead of the time when level pressing event occurs, while high frequency bands appear the opposite way.

high frequency bands contained more information while redundancy was involved in most low frequencies. The results in Figure 2 have shown that high frequencies components of LFP are useful to neural decoding, and the low coherence intensity of high frequency bands further indicates that complementary information among different LFP channels and multi-channel decoding is necessary.

B. Feature Extraction

Following the section A analyzed characteristic of LFP, the LFP signals of 16 channels were decomposed into 8

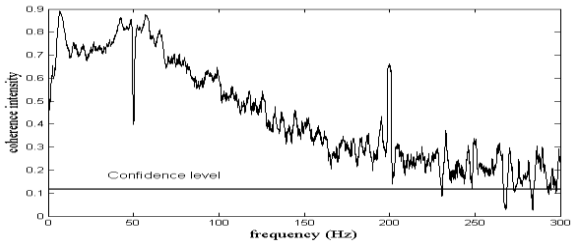

Fig. 3. LFP-LFP coherence of different frequency bands. The solid black line indicate the confidence level, the trend shows that there exists high correlation in low frequency bands. In contrast, the coherence dramatically falls to the confidence level with frequency increase, suggesting high frequency bands carry more information with less redundancy.

frequency bands using the method described in the section C. The data were binned with a 100ms bin, and 400ms time lag was used in our work, thus one feature at each bin increased to five. Therefore a large number of feature dimensions were obtained, which equals to 8×16×5=640. In this case high dimensional data were to deal with, the traditional decoding algorithms such as WF or KF were not suited.

C. Comparison of three decoding algorithms

The decoding performances of three algorithms mentioned were compared in Fig. 4, namely, PLSR, WF and KF. We evaluated the performance by the means of MSE and CC, which showed different results. The results in upper section illustrates PLSR occupied the lowest MSE in the three decoding methods. MSE of Wiener Filter was the

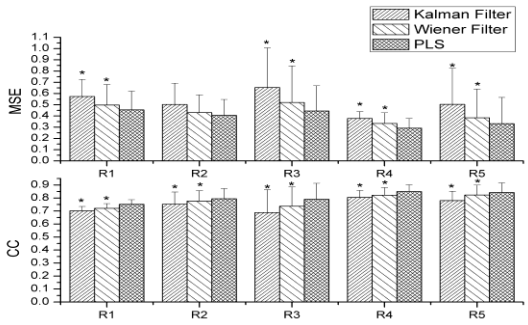

Fig. 4.The decoding performance was evaluated by CC and MSE. PLSR is optimal decoding algorithm of the three. The highest CC and lowest MSE were acquired with all time-frequency features of LFP by means of PLSR. Error bars represent the standard deviation of CC and MSE. The asterisk upper the bar shows these MSE and CC of three algorithms has significant difference (Friedman test $p < 0.05$).

second lowest, while Kalman Filter was the poorest performer. The bar chart of mean CC also showed that CC values ascended for all the rats when the algorithm used was PLSR. Kalman Filter, by contrast, performed less than the other two methods with the lowest values. Friedman test was used to test whether the difference of CC and MSE between three algorithms were significant. An asterisk upper the data bar symbolized significant difference of results. Figure 4 illustrated the methods are significantly different, expect for the MSE of R2. Therefore, we reach to a conclusion that PLSR can decode the neural activity as well as two common algorithms and even better in the case that all frequency bands were used.

Figure 5 shows a segment of the normalized pressure value and the corresponding LFP decoding algorithms, and corresponding average CC values were calculated. From the figure it can be clearly seen that prediction by WF and PLSR

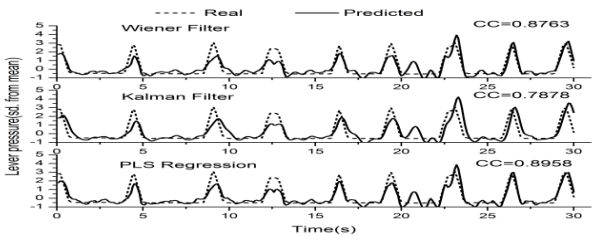

Fig. 5.Pressure values were predicted by WF, KF and PLSR using all time-frequency features. The actual (dash line) and decoded (solid line) pressure value were demonstrated in a normalized scale. The predicated trajectories and CC values show that PLSR has the best performance.

show good agreement with the experimental results, not merely peak time but also amplitude. Besides, the CC values are considerable high, both more than 0.8, especially of PLSR as high as 0.8958. Nevertheless, the cases of KF were quite different from those of WF and PLS Regression. The results shows that time delay can be obviously observed in KF prediction. It can be concluded that PLSR received the

most accurate results, while KF was inferior to the other two algorithms.

The average number of latent factors reflects the capacity of over-fitting avoidance and computational complexity of a model. Selected by PLSR and PCA, they were computed and compared. The information contained in the two tables (table I and table II) explains that the average extracted features of data differed greatly in quantity. Table I shows as a result of employing PLSR the number of latent factors explaining the output reduced sharply, whose model may be capable of reserving the optimal features relevant to the behavior. The number reached as low as 6.50 in R2, even the highest was only 10.20, which was far less than the original

TABLE I
PLSR OPTIMAL LATENT FACTORS AVERAGE NUMBER AND STANDARD DEVIATION

	R1	R2	R3	R4	R5
OLFAN	10.20	6.50	8.70	8.50	7.70
SD	4.42	4.09	5.29	5.13	4.62

OLFAN stands for optimal latent factors average.

TABLE II
PCA LATENT FACTORS AVERAGE NUMBERS CONTAINING 90% INFORMATION

	R1	R2	R3	R4	R5
LFAV	75.10	90.30	89.60	80.30	42.80
SD	0.57	0.48	0.52	0.67	1.23

LFAV stands for latent factors average numbers which contains 90% information.

number. However, seen from the table 2, even after PCA had diminished the redundancy, there remained a large amount of latent factors, and even the minimum was as many as 42.8000 that were relatively in large quantities versus the PLSR results. We can draw a conclusion that both PLSR and PCA were able to decrease the variation dimension, but PLSR exceled PCA in the level of feature reduction by the comparison of results.

IV. DISCUSSION AND CONCLUSION

In this paper we studied the characteristics of LFP signal. Spectrum analysis showed that high frequency bands took much information about kinematic parameters, although most of the energy of LFP signal was carried by low frequency bands. It suggested that multi-frequency bands decoding is necessary. Coherence analysis of LFP shows that less redundancy existed in high frequency components between different channels. These data implied that multi-channel decoding was necessary.

The necessity of multi-frequency bands and multi-channel decoding leads to a large number of feature dimensions of the decoding inputs. However, traditional decoding algorithms such as WF and KF have great risk of over-fitting, and especially are very time-consuming. These methods indeed can effectively avoid over-fitting by implementations such as regularizations or be estimated with subspaces. However, these implement methods still have no functions of choosing the optimal latent factors and reducing the input feature dimension, whereas PLSR can. Even though we applied PCA analysis to degrade the feature dimension, they still did not perform as well as PLSR did. The outperformances of PLSR were demonstrated in two aspects in our study. One was that the number of latent factors extracted by PLSR was much smaller than that of PCA components. Therefore, PLSR had the advantages of the better ability of the better capability of over-fitting avoidance and less computational complexity. Furthermore PLSR has a great advantage in noise removal, due to it is a supervised method which only extracts the latent factors related to the target motion parameter.

ACKNOWLEDGMENT

The authors are indebted to Dr. Junming Zhu and Chaonan Yu for exceptional technical assistance.

REFERENCES

[1] J.P. Donoghue, "Bridging the brain to the world: a perspective on neural interface systems," *Neuron*, vol. 60, (no. 3), pp. 511-21, Nov 6 2008.

[2] M.A. Lebedev and M.A. Nicolelis, "Brain-machine interfaces: past, present and future," *Trends Neurosci*, vol. 29, (no. 9), pp. 536-46, Sep 2006.

[3] L.R. Hochberg, M.D. Serruya, G.M. Friehs, J.A. Mukand, M. Saleh, A.H. Caplan, A. Branner, D. Chen, R.D. Penn, and J.P. Donoghue, "Neuronal ensemble control of prosthetic devices by a human with tetraplegia," *Nature*, vol. 442, (no. 7099), pp. 164-171, Jul 13 2006.

[4] J. Wessberg, C.R. Stambaugh, J.D. Kralik, P.D. Beck, M. Laubach, J.K. Chapin, J. Kim, S.J. Biggs, M.A. Srinivasan, and M.A. Nicolelis, "Real-time prediction of hand trajectory by ensembles of cortical neurons in primates," *Nature*, vol. 408, (no. 6810), pp. 361-5, Nov 16 2000.

[5] D.M. Taylor, S.I.H. Tillery, and A.B. Schwartz, "Direct cortical control of 3D neuroprosthetic devices," *Science*, vol. 296, (no. 5574), pp. 1829-1832, Jun 7 2002.

[6] M. Velliste, S. Perel, M.C. Spalding, A.S. Whitford, and A.B. Schwartz, "Cortical control of a prosthetic arm for self-feeding," *Nature*, vol. 453, (no. 7198), pp. 1098-1101, Jun 2008.

[7] J.C. Sanchez, J.C. Principe, T. Nishida, R. Bashirullah, J.G. Harris, and J.A.B. Fortes, "Technology and signal processing for brain-machine interfaces," *Ieee Signal Proc Mag*, vol. 25, (no. 1), pp. 29-40, Jan 2008.

[8] J. Zhuang, W. Truccolo, C. Vargas-Irwin, and J.P. Donoghue, "Decoding 3-D reach and grasp kinematics from high-frequency local field potentials in primate primary motor cortex," *IEEE Trans Biomed Eng*, vol. 57, (no. 7), pp. 1774-84, Jul 2010.

[9] A.K. Bansal, C.E. Vargas-Irwin, W. Truccolo, and J.P. Donoghue, "Relationships among low-frequency local field potentials, spiking activity, and 3-D reach and grasp kinematics in primary motor and ventral premotor cortices," *Journal of Neurophysiology*, 2011.

[10] J.M. Antelis, L. Montesano, and J. Minguez, "Decoding of full 3D finger trajectories from EEG data " *International Journal of Bioelectromagnetism* vol. 13, 2011.

[11] Z.C. Chao, Y. Nagasaka, and N. Fujii, "Long-term asynchronous decoding of arm motion using electrocorticographic signals in monkeys," *Frontiers in Neuroengineering*, vol. 3, 2010.

[12] S. Zhang, J. Bo, J. Zhu, Q. Zhang, W. Chen, X. Zheng, and T. Zhao, "A study on Combining Local Field Potential and Single Unit Activity for Better Neural Decoding," *International Journal of Imaging System and Technology*, vol. 21, pp. 165-172, 2011.

[13] P. Geladi and B. Kowalski, "Partial least-squares regression: a tutorial," *Analytica Chimica Acta*, vol. 185, pp. 1-17, 1986.

[14] W. Wu, A. Shaikhouni, J.P. Donoghue, and M.J. Black, "Closed-loop neural control of cursor motion using a Kalman filter," *P Ann Int Ieee Embs*, vol. 26, pp. 4126-4129, 2004.